# AMB controller design for a machining spindle using $\mu-$synthesis


Jerzy T. Sawicki
Dept. of Mechanical Engineering
Cleveland State University
2121 Euclid Avenue, SH 245
Cleveland, OH 44115
j.sawicki@csuohio.edu

Eric H. Maslen
Dept. of Mech. and Aero. Engrg.
University of Virginia
122 Engineer's Way
Charlottesville, VA 22904 USA
ehm7s@virginia.edu

Kenneth R. Bischof
Manufacturing Technology Development
Federal-Mogul Corporation
3935 Research Park Drive
Ann Arbor, Michigan 48108
Ken.Bischof@federalmogul.com



***Abstract*— Control of an AMB supported machining spindle was explored to determine the potential advantages of $\mu-$synthesis relative to more a conventional strategy based on PID with notch filters. The spindle was manufactured by Revolve Magnetic Bearings, Inc. and adapted to permit control using a dSpace real time digital controller. This very open platform enabled introduction of arbitrary control algorithms, synthesized in MatLab™.**

**The study compares the performance of a carefully designed PID + notch compensator to that of a $\mu-$synthesized controller. The main finding is that $\mu-$synthesis is better able to reduce tool tip compliance than is PID+notch and that this improvement was a factor of at least 2 over a wide range of frequencies for the spindle examined.**


## I. Introduction

As the application of High Speed Machining (HSM) in production environments grows, interest in the AMB machining spindles also increases (e.g., [1], [2], [3]). AMBs permit a higher bearing surface speed and larger diameter, or stiffer, spindle rotors. In addition, active control capabilities enable greater spindle damping and the active suppression of chatter [3].

However, to ensure high-quality machining operation, the advanced control strategies require an accurate mathematical model for the spindle, its components, as well as for the cutting dynamics. This paper presents a modeling approach for a high-speed spindle-bearing system based on finite-element analysis coupled with experimental modal identification and compares the performance of controllers synthesized with the resulting model.

## II. AMB Spindle and Model

The platform for this study is an AMB supported machine tool spindle with the cross section shown in Figure 1. The spindle was originally developed by Revolve Magnetic Bearings, a subsidiary of SKF, Inc., and adapted to permit control using a dSPACE digital controller. The spindle rotor is supported by two radial bearings and one thrust bearing. The maximum static radial load capacities are approximately 1400 and 600 N for the front and rear bearings, respectively, and the maximum axial capacity for thrust bearing is 500 N. The spindle reaches a rotational

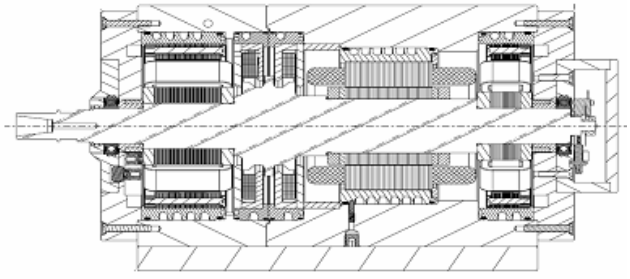

Fig. 1. Cross section of AMB machining spindle without tool holder.

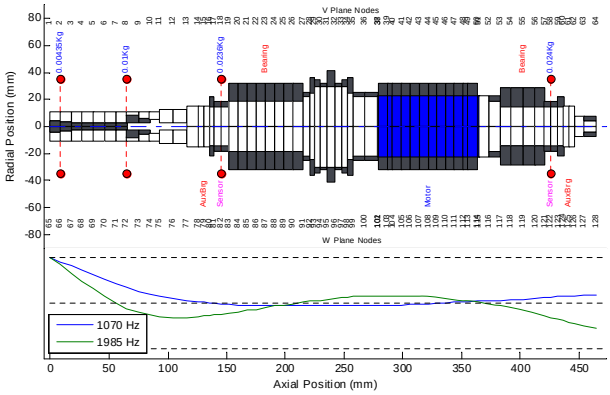


Fig. 2. Finite element model and first two bending modes of free-free rotor with tool holder.

speed of 50,000 rpm at 10 kW. The AC motor acts on the rotor between the thrust and rear radial bearing.

A free-free rotor model was constructed using a Timoshenko beam element formulation containing 64 elements. Proportional damping and linear gyroscopic effects were assumed. The large rotor model was then reduced using modal reduction to four principal modes, including the two rigid body modes. Figure 2 shows the rotor finite element model and the first two bending modes.

A PID controller was designed to perform a system identification of the levitated spindle to experimentally determine the closed-loop transfer function between current disturbance and rotor response. The modeled Bode plot

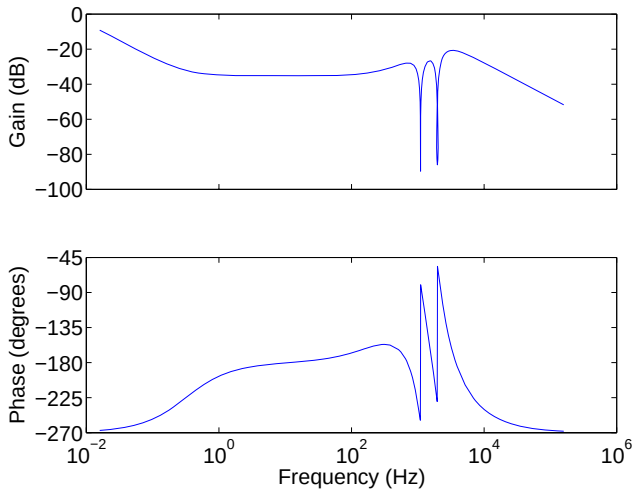


Fig. 3. Modeled transfer function of PID controller. All four diagonal (direct) elements are the same: all off-diagonal (cross coupling) elements are zero.

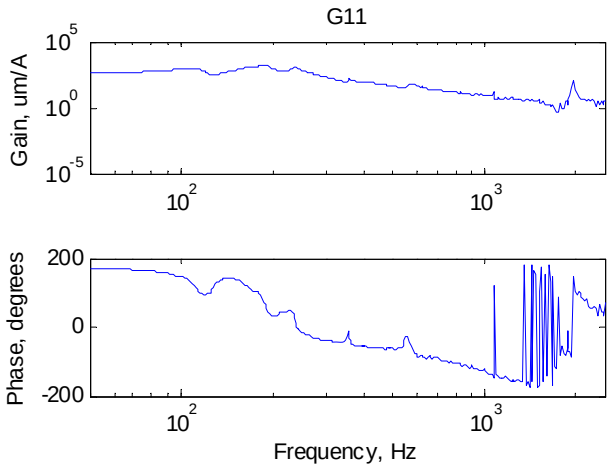


Fig. 4. Experimentally extracted closed-loop transfer function of the system with the PID controller depicted in Figure 3.

for the controller implemented at 10 kHz is shown in Figure 3. With the levitating controller operating, a sine sweep current signal (0.25 Ampere over a 0 to 2500 Hz frequency bandwidth) was injected to each axis at a time and closed-loop performance was extracted. Figure 4 illustrates the results of such measurement when the current perturbation and measurement are taken for the same axis at the front bearing. A linearized AMB model was employed, and the parameters of the AMB were obtained from the analytical model and subsequently refined using the closed-loop testing data.

The controller was implemented using dSPACE based on differential control, with 10 output channels required and provided by the two D/A boards. The hardware consisted of the DS1005 PPC Board featuring the PowerPC 750GX running at 1Ghz. The controller sampling time was 10 kHz.

The resulting system model for controller synthesis and assessment is indicated in Figure 5. The available experimental and control inputs are indicated as $u$ while the

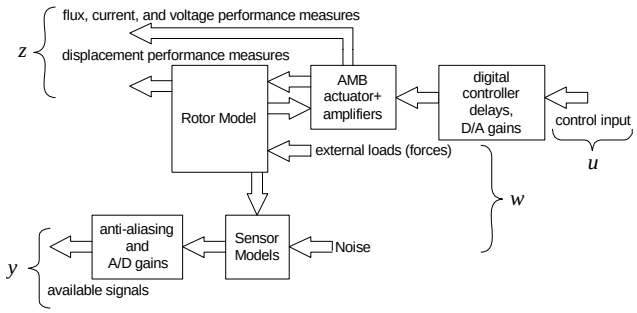


Fig. 5. Structure of the full model for controller synthesis and assessment.

available measurements are indicated as $y$. Other signals (loads, noise) acting on the system are indicated as $w$ while the quantities that form performance assessment such as peak rotor displacement, peak amplifier voltage, peak coil current, and peak magnetic flux are indicated collectively as $z$. The control goal, of course, is to use measurements $y$ to guide control efforts $u$ to make responses $z$ to loads $w$ *acceptable*.

Figure 6 presents a comparison of two of the 16 components of the open loop plant transfer function extracted experimentally and the plant model with the amplifier bandwidth set to 2475 Hz and the sample delay set to 170 microseconds. The first bending mode at 1970 Hz is nearly indistinguishable in a plot of $G_{11}$ due to the presence of a node for the first mode that is very close to the sensor location.

To obtain this open loop transfer function in a MIMO system like an AMB supported rotor, some care must be taken in the signal processing. In this case, the system has four inputs (amplifier perturbations for the $x-$ and $y-$ axes of each bearing plane) and four outputs (sensor signals for the $x-$ and $y-$ axes of each sensing plane). Thus, the open loop transfer function has the form:

$$\begin{bmatrix} y_1 \\ y_2 \\ y_3 \\ y_4 \end{bmatrix} = G(s) \begin{bmatrix} u_1 \\ u_2 \\ u_3 \\ u_4 \end{bmatrix}$$

in which $G(s)$ is a $4 \times 4$ matrix of transfer functions.

To measure $G(s)$, we conduct 4 experiments in which each of the input signals $u_i$ is perturbed individually. That is, for the first experiment, we inject a sinusoidal perturbation to $u_1$, for the second, to $u_2$ and so on. For each conducted experiment, a vector of *all* inputs to the plant and a vector of all outputs from the plant were recorded. That is, at each frequency, four sets of Fourier coefficients were measured for the four amplifier inputs and four sensor outputs:

$$\mathbf{U}(\omega_i) = \begin{bmatrix} U_{1,1}(\omega_i) & U_{1,2}(\omega_i) & U_{1,3}(\omega_i) & U_{1,4}(\omega_i) \\ U_{2,1}(\omega_i) & U_{2,2}(\omega_i) & U_{2,3}(\omega_i) & U_{2,4}(\omega_i) \\ U_{3,1}(\omega_i) & U_{3,2}(\omega_i) & U_{3,3}(\omega_i) & U_{3,4}(\omega_i) \\ U_{4,1}(\omega_i) & U_{4,2}(\omega_i) & U_{4,3}(\omega_i) & U_{4,4}(\omega_i) \end{bmatrix}$$

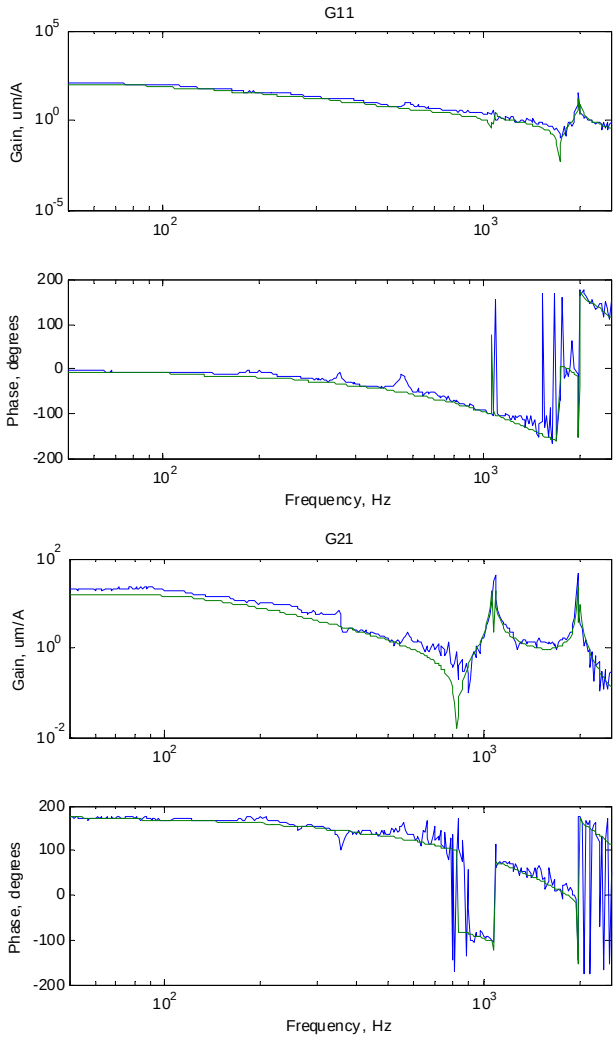


Fig. 6. Comparison of the modeled and experimentally extracted open loop transfer function of the plant.

$$\mathbf{Y}(\omega_i) = \begin{bmatrix} Y_{1,1}(\omega_i) & Y_{1,2}(\omega_i) & Y_{1,3}(\omega_i) & Y_{1,4}(\omega_i) \\ Y_{2,1}(\omega_i) & Y_{2,2}(\omega_i) & Y_{2,3}(\omega_i) & Y_{2,4}(\omega_i) \\ Y_{3,1}(\omega_i) & Y_{3,2}(\omega_i) & Y_{3,3}(\omega_i) & Y_{3,4}(\omega_i) \\ Y_{4,1}(\omega_i) & Y_{4,2}(\omega_i) & Y_{4,3}(\omega_i) & Y_{4,4}(\omega_i) \end{bmatrix}$$

In this manner, the signals are expected to be related by

$$\mathbf{Y}(\omega_i) = G(j\omega_i)\mathbf{U}(\omega_i)$$

and the transfer function may be obtain by the simple arithmetic

$$G(j\omega_i) = \mathbf{U}^{-1}(\omega_i)\mathbf{Y}(\omega_i)$$

If the perturbations for the four experiments have been chosen well, then the required inverse $\mathbf{U}^{-1}(\omega_i)$ will exist all all of the test frequencies.

## III. $\mu$-SYNTHESIS BASED CONTROLLER

$\mu$-synthesis is a model-based controller design technique requiring an accurate mathematical model of the plant dynamics and bounds on the uncertainties associated with that model [4]. This design methodology, focused on achieving guaranteed stability and performance for uncertain systems, can be very effective for machining application, due to the presence of variation of cutting forces, feed rates, and various cutting conditions.

The starting point for $\mu-$ synthesis is a model such as that depicted in Figure 5, but this must be extended to include weighting functions and uncertainty specifications.

### A. Weighting functions

The purpose of the weighting functions is to normalize the performance ($z$) and load ($w$) signals, with the goal of making the maximum expected magnitude of $w$ be 1.0 (no units) at all frequencies and the maximum allowed magnitude of $z$ be 1.0, also at all frequencies. As an example, if $w_1$ is an unbalance with mass eccentricity not to exceed 0.1 g-mm, then

$$|w_1| \leq 1 \times 10^{-7}\omega^2$$

Thus, we can normalize $w_1$ by

$$\overline{w}_1 = \frac{1}{10^{-7}s^2} w_1$$

For an input signal, the weighting function converts a normalized signal to the physical signal:

$$w = W_w \overline{w}$$

so that, for this example, the ideal weighting function would be

$$W_{w,1}(s) = 10^{-7}s^2$$

In practice, we require that the weighting functions are strictly proper so that they can be represented with a state space model. In this case, if the rotor will never be operated above some speed $\omega \leq \omega_{\max}$, then the weighting function may be made strictly proper by

$$W_{w,1}(s) = \frac{10^{-7}s^2}{(s/2\omega_{\max})^2 + \sqrt{2}s/2\omega_{\max} + 1}$$

which gives a good approximation to $10^{-7}s^2$ out to $\omega_{\max}$.

For an output signal, the weighting function converts the physical performance measure back to a normalized measure:

$$\overline{z} = W_z z$$

The simplest example of this is a clearance limitation. Assume that $z_1$ measures the displacement of the rotor at some point where there is potential contact between the rotor and the casing. If the clearance is 0.5 mm and $z_1$ is measured in meters, then

$$\overline{z}_1 = \frac{1}{0.0005} z_1$$

As long as $|\overline{z}_1| < 1$, then $|z_1| < 0.5$ mm, as required. Thus,

$$W_{z,1} = \frac{1}{0.0005}$$

which is not frequency dependent.

In this manner, weighting functions are selected for each component of $w$ and $z$ so that the performance of the system is judged to be acceptable if

$$\overline{z} = W_z z \ : \ |\overline{z}| < 1 \ \forall \ |\overline{w}| < 1 \ : \ w = W_w \overline{w}$$

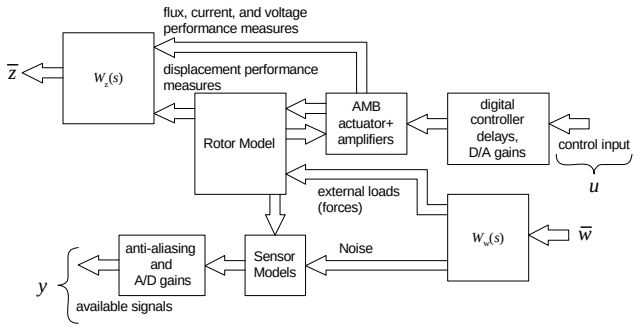


Fig. 7. Weighted model: weighting functions $W_w$ and $W_z$ normalize the load and performance signals.

TABLE I
BEARING LOAD PARAMETERS

| | tool tip end | drive end |
|---|---|---|
| DC load | 300 N | 130 N |
| first break | 0.001 Hz | 0.001 Hz |
| midfrequency load | 80 N | 50 N |
| second break | 40 Hz | 40 Hz |

The resulting modified (weighted) plant model is shown in Figure 7.

For the machine tool spindle problem, the loads were assumed to act at the bearing locations while each of the position sensors was assumed afflicted with noise. The bearing loads are summarized in Table I while the sensor noise was 0.6 micrometers broad-band. The performance measures included amplifier voltage (limited to 300 volts), coil current (limited to 7 amps above a 5 amp bias), and journal displacement at the two bearing locations (limited to 50 micrometers at frequencies above 0.002 Hz, and 0.5 micrometers below this).

### *B. Uncertainty*

A significant goal of $\mu-$synthesis is to design controllers which are robust to variations in plant dynamics. A simple example is the effect of gyroscopics: the dynamics of the rotor at standstill are substantially different from those observed when spinning at 16000 RPM. The rotor model contains the rotor spin rate explicitly:

$$M\ddot{x} + [D + \Omega G]\dot{x} + Kx = f$$

in which the gyroscopic behavior of the rotor mass is represented by the matrix $G$ and $\Omega$ is the spin speed of the rotor. If a controller is designed for the rotor with $\Omega = 0$, then there may be no guarantee that the system will be stable for other values of $\Omega$: obviously undesirable.

In the $\mu-$ framework, uncertainties are represented as feedback gains connected to the plant where the nominal value of the feedback gain is zero but it is understood that the gain could lie anywhere inside a real range or complex disk. By convention, the size of this range is chosen to be 1.0. As an example, suppose that our rotor had a seal acting at some location along the shaft. The seal might have some nominal cross-coupled stiffness of 1000 N/m

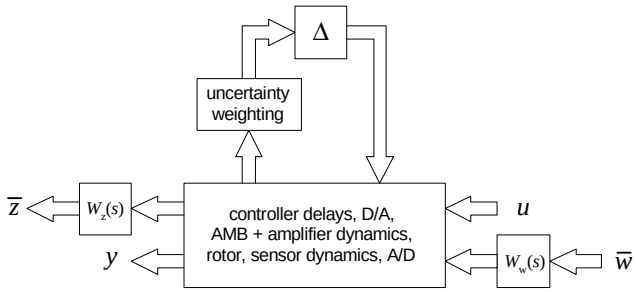


Fig. 8. Model with weighting functions and uncertainty added.

but with uncertainty of $\pm 300$ N/m:

$$\begin{bmatrix} f_{s,x} \\ f_{s,y} \end{bmatrix} = \begin{bmatrix} 0 & 1000 \pm 300 \\ -1000 \mp 300 & 0 \end{bmatrix} \begin{bmatrix} x \\ y \end{bmatrix}$$

This can be represented by

$$\begin{bmatrix} f_{s,x} \\ f_{s,y} \end{bmatrix} = \begin{bmatrix} 0 & 1000 \\ -1000 & 0 \end{bmatrix} \begin{bmatrix} x \\ y \end{bmatrix} + 300 \begin{bmatrix} 0 & \pm 1 \\ \mp 1 & 0 \end{bmatrix} \begin{bmatrix} x \\ y \end{bmatrix}$$

The first part of the relationship defines the *nominal* behavior and would be included in the core model. The second part defines a feedback with nominal value of zero. The scale 300 N/m would be applied to the input or output matrices tying this feedback into the rotor model and the remnant would be the uncertainty matrix, denoted $\Delta$.

The product of adding weighting functions and uncertainty representations to the base model is depicted in Figure 8.

For the machine tool spindle, the primary uncertainties were judged to be actuator properties, modal properties for the two bending modes retained, and, of course, rotor speed. The uncertainties in actuator gain and bearing negative stiffness were modeled as 3% and 15% real uncertainties of nominal value, respectively. The modal frequencies of the first and second modes were modeled as 1% complex uncertainty of nominal value for each mode. These latter uncertainties discourage the synthesis machinery from introducing controller dynamics that precisely cancel the dynamics associated with these modes as, for instance, very sharp notch filters. Rotor speed was modeled as 8000 RPM with an uncertainty of 100% in order to obtain a stabilizing controller for the speed range from 0 to 16000 RPM.

### *C. Synthesis*

Several $\mu$-controllers were designed and just two examples are illustrated in Figure 9, where one of the controllers was optimized to achieve the best machining performance in terms of high surface finish quality. Both controllers were implemented as discrete time, state-space systems with a sampling rate of 10 kHz. For each case the MatLab$^{TM}$ Robust Control Toolbox was used to synthesize robust controller via -synthesis D-K iteration. The resulting optimized controller was 88th order and was reduced to

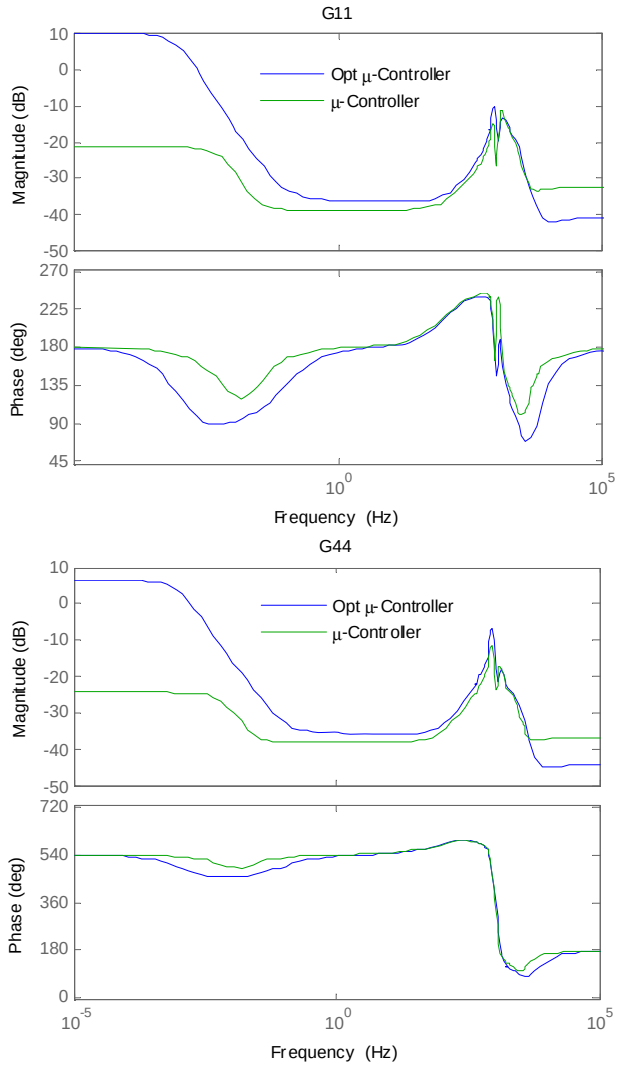


Fig. 9. Comparison of two $\mu$-controllers; one is optimized for machining.

44th order by model order reduction using Hankel singular value based algorithms. Differences between the controllers were generated by changing the performance and load weighting functions.

To determine the spindle stiffness at the tool tip, with the rotor supported on each the PID, the $\mu$-controller, and the optimized $\mu$-controller, impact testing was carried out with an instrumented hammer. The results presented in the upper plot of Figure 10 show the advantage of $\mu$-controllers, especially in the vicinity of the first and second modes, where the PID stiffness is significantly lower. Over the wide range of frequencies the PID controller is much less stiff while the optimized $\mu$-controller provides the highest stiffness. This is illustrated on the spindle stiffness at the tool tip plot for the optimized $\mu$-controller normalized with respect to the stiffness of the corresponding PID controller, as shown in the bottom plot of Figure 10.

## IV. Conclusions

The presented simulation and experimental results show the potential of $\mu$-synthesized control of AMB machining

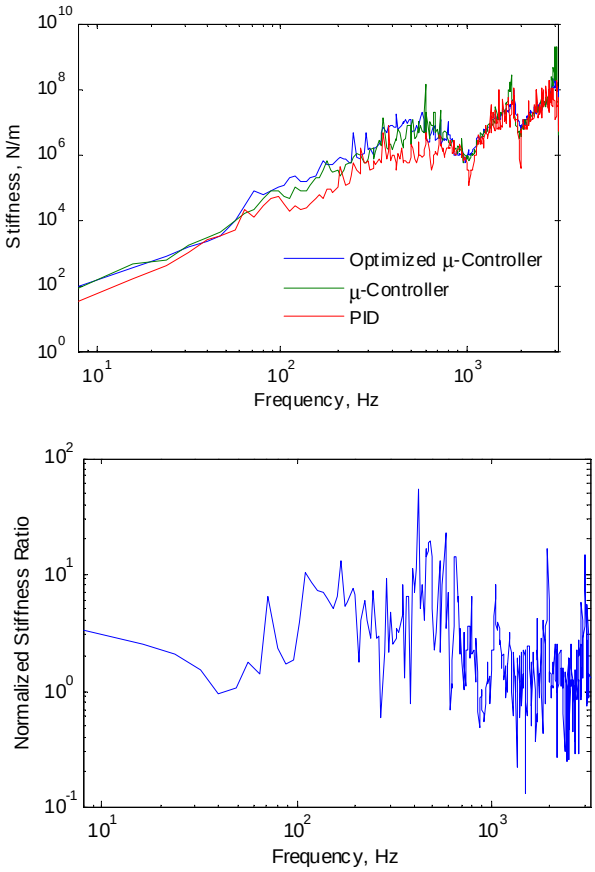


Fig. 10. Stiffness of the spindle at the tool tip extracted from the hammer test for PID and $\mu-$controllers (upper plot); normalized with respect to PID optimized $\mu$-controller stiffness.

spindles for improved cutting performance. In particular, the $\mu$-controllers were able to realize substantially higher broad-band spindle tip stiffness that could be achieved (through manual tuning) by the PID + notch controller.

Perhaps a more important advantage is the structure of the synthesis process provided by $\mu-$synthesis. In particular, the synthesis outcome is guided by choice of performance functions and load models and the resulting closed loop performance reflects these functions in a direct manner. Consequently, there is less need for synthesis tricks with the $\mu-$ approach. Further, the $\mu-$ approach provides a convenient and rational repository for accumulating system knowledge through model and weighting function refinement. Finally, the $\mu-$ approach can provide guarantees of robustness to wide ranges of system parameter such as the operating speed range without requiring gain scheduling or other special techniques: all $\mu-$synthesized controllers developed in the course of this study were stable over the entire operating range while agressive PID + notch designs did not reliably meet this requirement.

## References

[1] Siegwart, R., Larsonneur, R., and Traxler, A., 1990, "Design and Performance of a High Speed Milling Spindle in Digitally Controlled Active Magnetic Bearings," 2nd International Symposium on Magnetic Bearings, Tokyo, Japan, pp. 197-204.

[2] Fittro, R., Hammond, R., Allaire, P., and Maslen, E., 1997, “Initial Controller Design of a Magnetic Bearing Supported Prototype Textile Spindle,” Proceedings of MAG ’97 Industrial Conference and Exhibition on Magnetic Bearings, Alexandria, VA, pp. 57-65.
[3] Fittro, R. L. and Knospe, C.R., 1998, “$\mu$-Synthesis Control Design Applied to a High Speed Machining Spindle With Active Magnetic Bearings,” 6th International Symposium on Magnetic Bearings, MA, USA, pp. 449-458.
[4] Zhou, K. and Doyle, J., 1998, *Essentials of Robust Control*, Prentice-Hall, Upper Saddle River, NJ.